Pharmaceutical Research, Vol. 22, No. 10, October 2005 (© 2005)
DOI: 10.1007/s11095-005-6627-z

Research Paper

The Steady-State Michaelis–Menten Analysis of P-Glycoprotein Mediated Transport Through a Confluent Cell Monolayer Cannot Predict the Correct Michaelis Constant K_m

Joe Bentz,[1,5] Thuy Thanh Tran,[1,2] Joseph W. Polli,[3] Andrew Ayrton,[4] and Harma Ellens[2]

Received March 24, 2005; accepted June 14, 2005

Purpose. Typically, the kinetics of membrane transport is analyzed using the steady-state Michaelis–Menten (or Eadie–Hofstee or Hanes) equations. This approach has been successful when the substrate is picked up from the aqueous phase, like a water-soluble enzyme, for which the Michaelis–Menten steady-state analysis was developed. For membrane transporters whose substrate resides in the lipid bilayer of the plasma membrane, like P-glycoprotein (P-gp), there has been no validation of the accuracy of the steady-state analysis because the elementary rate constants for transport were not known.
Methods. Recently, we fitted the mass action elementary kinetic rate constants of P-gp transport of three different drugs through a confluent monolayer of MDCKII-hMDR1 cells. With these elementary rate constants in hand, we use computer simulations to assess the accuracy of the steady-state Michaelis–Menten parameters. This limits the simulation to parameter ranges known to be physiologically relevant.
Results. Using over 2,300 different vectors of initial elementary parameters spanning the space bounded by the three drugs, which defines 2,300 "virtual substrates", the concentrations of substrate transported were calculated and fitted to Eadie–Hofstee plots. Acceptable plots were obtained for 1,338 cases.
Conclusion. The fitted steady-state V_{max} values from the analysis correlated to within a factor of 2–3 with the values predicted from the elementary parameters. However, the fitted K_m value could be generated by a wide range of underlying "molecular" K_m values. This is because of the convolution of the drug passive permeability kinetics into the fitted K_m. This implies that K_m values measured in simpler systems, e.g., microsomes or proteoliposomes, even if accurate, would not predict the K_m values for the confluent monolayer system or, by logical extension, *in vivo*. Reliable *in vitro–in vivo* extrapolation seems to require using the elementary rate constants rather than the Michaelis–Menten steady-state parameters.

KEY WORDS: elementary rate constants; Michaelis–Menten; P-gp; pharmacokinetic extrapolation; transcellular transport.

INTRODUCTION

The clinical and biological relevance of the human multidrug resistance transporter P-glycoprotein (P-gp) has been demonstrated through a large number of *in vitro*, preclinical, and clinical studies (1–6). A variety of *in vitro* expression systems have been used to study P-gp: suspension cells overexpressing P-gp, lipid reconstitutions of purified P-gp, plasma membrane vesicles, and more recently confluent cell monolayers (7–24).

Kinetic studies of P-gp transport have been analyzed using versions of the steady-state Michaelis–Menten analysis (12,13,16–19,21,25–32). Although the fitted V_{max}, K_m, and sometimes a "Hill" number are acknowledged as phenomenological coefficients, the implicit assumption is that these fitted parameters correlate reasonably well with the molecular values defined by the elementary rate constants of the transporter reaction, according to the classical Michaelis–Menten derivation (33). Otherwise, the fitted values would have no physical significance and little predictive value.

The Michaelis–Menten analysis was developed for soluble enzymes, which bind substrate directly from the aqueous phase to which the substrate is added initially. Therefore, it applies well enough to membrane transporters, which bind their substrate directly from the water phase, e.g., glucose permeases (25). It seems to apply to the ATPase

[1] Department of Bioscience and Biotechnology, Drexel University, Philadelphia, Pennsylvania 19104, USA.
[2] Preclinical Drug Metabolism and Pharmacokinetics, GlaxoSmithKline, King of Prussia, Pennsylvania 19406, USA.
[3] Preclinical Drug Metabolism and Pharmacokinetics, GlaxoSmithKline, Research Triangle Park, North Carolina 27709, USA.
[4] Preclinical Drug Metabolism and Pharmacokinetics, GlaxoSmithKline, Welwyn, UK.
[5] To whom correspondence should be addressed. (e-mail: bentzj@drexel.edu)

ABBREVIATIONS: A > B (or B > A), transport across the confluent cell monolayer when the donor chamber is apical (or basolateral) and the receiver chamber is basolateral (or apical); P-gp, the P-glycoprotein product of the hMDR1 gene.

activity of P-gp because that activity resides in the cytosolic domain of P-gp (7,10,12,14,15,20–22), even after detergent reconstitution (34). However, P-gp picks up drugs from the inner apical monolayer of the cell (35), which is a permeation barrier away from substrate added to either face of a confluent cell monolayer.

For the confluent cell monolayer system, evaluation of the correlation between the steady-state parameters and the underlying elementary rate constants can be performed using computer simulations, i.e., where model transport data are calculated according to known elementary rate constants and other parameters relevant to this expression system. When these model data are fitted to an Eadie–Hofstee plot, the validity of the correlation would be known. To date, this simulation has not been performed, perhaps because the potential parameter space for the elementary rate constants is immense (24). It is almost *a priori* likely that in some parameter domains, the correlation would be good, and in other parameter domains, it would be poor. Without knowledge of which domains were physiologically relevant, the computational exercise would have little significance.

In Tran *et al.* (24), we fitted the elementary rate constants, passive permeability coefficients, and estimates for partition coefficients for P-gp transport experiments using MDCKII-hMDR1 cell monolayers for the P-gp substrates amprenavir (an HIV protease inhibitor), quinidine (a Na^+ channel blocker), and loperamide (an antidiarrheal drug). These physiologically relevant elementary parameters permit us to construct a parameter domain space, bounded by the specific values for the three drugs, within which we can simulate model data and test the accuracy of the steady-state analysis.

We show here that if P-gp mediated transport in the confluent monolayer system is as simple as modeled and fitted in Tran *et al.* (24), the steady-state analysis for the Michaelis constant K_m cannot be estimated accurately, even if the data have no error. Despite well-fitted Eadie–Hofstee plots, the estimated K_m value can be 2-3 orders of magnitude larger than the true molecular value, as calculated from the elementary rate constants used to generate the model transport data in the first place. If it turns out that the kinetic model of P-gp transport for the confluent cell monolayer system is more complex than our minimal model (24), as is likely to happen over time, then the Michaelis–Menten steady-state analysis would be even more inaccurate.

It is likely that the inherent inaccuracy of a fitted K_m would hold for any expression system, which has a permeability barrier between the P-gp binding site and the donor aqueous phase, e.g., suspension cells and "right side out" microsome and proteoliposome preparations. This has not been tested. Nevertheless, even if the K_m was accurately measured in one of these simpler systems, our results prove that this number cannot reliably predict the K_m, which would be found for the confluent monolayer system and, by extension, for tissue. This is true regardless of the additional complicating effects of lipid composition and membrane asymmetry on P-gp activity (40,41). Any extrapolation from *in vitro* data to *in vivo* transport must begin by using the elementary rate constants and associated parameters to have a hope for accuracy.

Understanding the mechanism of P-gp transport will require input from many expression systems, from the simplest purified protein reconstitution to the physiologically relevant confluent cell monolayers. Furthermore, each system must be analyzed by the most accurate kinetic expressions available. Otherwise, the kinetic analysis itself will obscure the mechanism.

MATERIALS AND METHODS

Materials

Amprenavir and GF120918 were from GlaxoSmithKline (Research Triangle Park, NC, USA). Loperamide was from Sigma (St. Louis, MO, USA) and quinidine from Fisher Scientific (Fair Lawn, NJ, USA). ^{3}H-Loperamide (10 Ci/mmol) and ^{3}H-amprenavir (21 Ci/mmol) were custom synthesized by Amersham Pharmacia Biotech (Little Chalfont, Buckinghamshire, England). ^{3}H-Quinidine (20 Ci/mmol) was from ICN Biomedical, Inc., Costa Mesa, CA, USA. Dimethyl sulfoxide was from Sigma-Aldrich, Deisenhofen, Germany. Dulbecco's Modified Eagle Medium (DMEM) was from MediaTech, VWR, Herndon, VA, USA. Transport medium (DMEM with 25 mM HEPES buffer, high glucose, L-glutamine, pyridoxine hydrochloride, without sodium pyruvate, and without phenol red) was from Gibco, Gaithersburg, MD, USA. Cholesterol and porcine brain lipids were from Avanti Polar Lipids, Inc. (Alabaster, AL, USA). Transwell 12-well plates with polycarbonate inserts were obtained from Costar (Acton, MA, USA). Ultima Gold scintillation cocktail was from PerkinElmer Life Sciences (Boston, MA, USA).

Compound Selection

These drugs were chosen because they are good P-gp substrates, are chemically unrelated, and show different mass balance problems (22). Furthermore, amprenavir shows no evidence for transport saturation (36), rendering the standard Michaelis–Menten analysis of P-gp transport useless.

Cell Line and Culture Conditions

The Madin–Darby Canine Kidney cell line, which overexpresses human MDR1 (MDCKII-hMDR1), was purchased from the Netherlands Cancer Institute (Amsterdam, Netherlands) (37). Cells were split twice a week and maintained in culture medium (DMEM supplemented with 10% fetal bovine serum, 50 U/ml penicillin, and 50 μg/ml streptomycin). Cells were kept at 37°C in 5% CO_2.

Transport Assays

Cells were seeded in 12-well plates at a density of 200,000 cells per insert and grown for 4 days in culture medium. Cells were given fresh media 1 day after seeding.

Prior to the experiment, culture medium was removed and cells were preincubated for 30 min with either transport medium alone (see above) or transport medium supplemented with 2 μM GF120918 to inhibit P-gp (36,38). Transport of a

range of concentrations of amprenavir, loperamide, and quinidine across the confluent monolayer of cells was measured in both directions, i.e., apical to basolateral (A > B) and basolateral to apical (B > A) in the presence and absence of GF120918. For incubations in the presence of GF120918, the inhibitor was added to both chambers. An amount of 0.5 μCi/ml of ^{3}H-amprenavir, ^{3}H-quinidine, or ^{3}H-loperamide was added to each respective drug concentration to allow quantification of transport from donor to receiver chambers by liquid scintillation counting. In addition, ^{14}C-mannitol (0.75 μCi/ml) was added to monitor cell monolayer integrity. At the indicated time points, 25-μL samples were taken from both donor and receiver chambers, mixed with 10 ml of Ultima Gold scintillation cocktail, and counted using a Hewlett Packard Liquid Scintillation Counter. The first time point taken was after 6 min, and we used these data as the starting point for fitting. This eliminated the need to correct for some drug binding to the Costar Transwell apparatus and other initial transient effects (23,24).

Cell Stability and Drug Metabolism

We showed that the stability of the cell monolayer and plasma membrane with respect to passive and active transport was not affected by the prolonged exposure times to amprenavir for at least 6 h (23). It was also shown that metabolism or decomposition was insignificant for all drugs on this time scale using radio-high-performance liquid chromatography.

Numerical Integrations

We used the stiffest integrator in MATLAB, ode23s, with absolute and relative tolerances set to 10^{-10}. Other MATLAB integrators, although faster, were not accurate enough at the later times of simulations.

Further details can be found in Tran *et al.* (23,24).

KINETIC MODEL OF TRANSPORT ACROSS A CONFLUENT CELL MONOLAYER

Figure 1 is a cartoon of a confluent cell monolayer, with P-gp (upward arrows) expressed on the apical surface. MDCKII-hMDR1 cells polarize with the basolateral membrane attached to the polycarbonate filters (39). The apical and basolateral chambers are kept separate by the tight junctions. Passive transport occurs and is separately analyzed using a potent P-gp inhibitor (24). Active transport by P-gp occurs vectorially, with substrate binding to a site on P-gp within the apical membrane inner monolayer and with efflux into the apical chamber (4,12,24,35). We can measure the concentration of substrate in the apical chamber, denoted C_A, and the basolateral chamber, denoted C_B. However, the concentration of substrate in the inner plasma membrane in contact with the P-gp binding site, denoted C_{PC}, cannot (yet) be measured rigorously in real time. All these concentrations are variables of the mass action model and fitted according to the measured values of C_B and C_A over time (24).

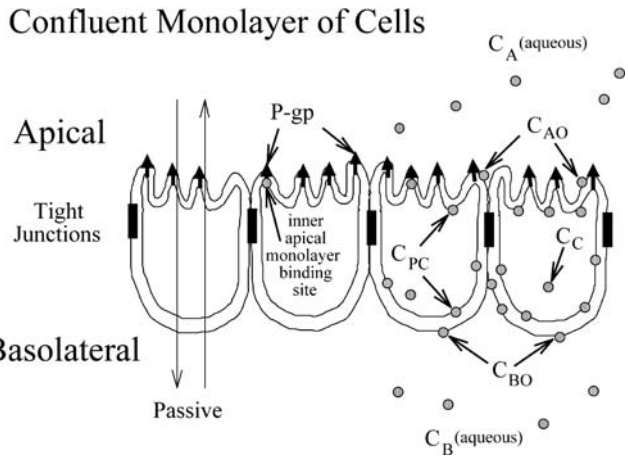

Fig. 1. Model of a confluent cell monolayer, with the apical membrane on top and the basolateral membrane on the bottom, where it binds to the polycarbonate insert. Passive permeability occurs in both directions. P-glycoprotein (P-gp) expressed on the apical membrane transports drug from the inner apical membrane monolayer into the apical chamber. The concentrations of drug in the apical and basolateral chambers, C_A and C_B, are measured, whereas the concentrations of drug in the inner plasma membrane, C_{PC}, and the cytosol, C_C, are predicted as part of the data fitting process described in Tran *et al.* [24].

We used the simplest Michaelis–Menten mass action reaction to model P-gp:

$$T_0 + C_{PC} \underset{k_r}{\overset{k_1}{\rightleftharpoons}} T_1 \xrightarrow{k_2} T_0 + C_A \tag{1}$$

where T_0 is the empty transporter, C_{PC} is the substrate in the apical membrane inner monolayer, T_1 is the transporter bound by substrate, and C_A is the substrate after efflux into the apical chamber. ATP hydrolysis is not part of this model because it occurs intracellularly and cannot (yet) be measured rigorously in real time. However, we found that the cells do not lose any capacity for drug transport over 6-h incubations (24) (Acharya and Bentz, unpublished data), implying that cellular ATP levels remain adequate for full P-gp function throughout the experiment.

Table I shows the mean consensus values of the elementary parameters used to fit the transport kinetics of amprenavir, quinidine, and loperamide (24). Each parameter fitted had a range that gave excellent fits to all the data for over 6 h of transport. The values shown in Table I are the mean values of the range.

Although the precision of these estimates varies by fitted parameter, that precision is not important for this work. We only use these mean values for each of the three drugs to create a boundary for the values of the "virtual substrates". If the values of the means shown in Table I were increased or decreased within their standard deviations, there would be no effect on our conclusions. The only important point is that the parameter values used here are physiologically relevant, and that this is not simply a theoretical "result".

We found that all three drugs had essentially the same rate constant for association to P-gp, denoted k_1, and essentially the same estimated surface density for efflux active P-gp, denoted $T(0)$, which was a benchmark for our

Table I. Parameter Values for Simulations[a]

Substrate	Efflux active P-gp density, $T(0)$[b] (P-gp/μm^2)	Association to P-gp, k_1[c] (M^{-1} s^{-1})	Efflux to apical chamber, k_2[d] (s^{-1})	Passive permeability coefficient, P[e] (nm/s)	Partition coefficient, K_{PC}[f]	Binding constant, K_B[g] (M^{-1})
AMP	40	$3 \times 10^{+9}$	200	200	200	1,300
QND	40	$3 \times 10^{+9}$	15	300	700	6,000
LPM	40	$3 \times 10^{+9}$	5	100	3,000	150
Simulation range used	40	$3 \times 10^{+9}$	2–400	50–1,000	100–5,000	100–10,000

[a] These are mean values obtained for each of the elementary parameters fitted in Tran *et al.* (24). Because we are using these values to simulate the transport of "virtual" substrates, whose physiochemical characteristics are defined between the drugs tested (amprenavir, quinidine, and loperamide), the error on the original fits is not relevant.

[b] Mean values for the density of efflux active P-gp in the apical membrane inner monolayer for each of the three drugs. As discussed in Tran *et al.* (24), this number can be roughly ten times smaller than the true surface density, perhaps due to the microvilli.

[c] Mean value for each of the three drugs. This is the rate constant from flip-flop across the basolateral membrane to association with the P-gp binding site. The route appears to be largely lateral diffusion controlled through the inner plasma monolayer, and the magnitude suggests that it is limited only by lipid lateral diffusion.

[d] Mean value for the efflux rate constant.

[e] This is the steady-state value for the drug's passive permeability coefficient. In reality, the passive permeability coefficients took from 15 min to 3 h to reach steady-state and $P(B > A)$ was not the same as $P(A > B)$ until their steady state was reached (23). Using these transient conditions would make the calculations and explanations much more complex, without changing any conclusions. We assumed the ideal situation of a static symmetric passive permeability barrier.

[f] In reality, three partition coefficients are needed to simulate model data: K_{PC} is between the cytosol and the inner plasma monolayer; K_{BO} is between the basolateral chamber and the outer basolateral monolayer; and K_{AO} is between the apical chamber and the outer apical monolayer. As explained in Tran *et al.* (24), direct measurements using cells would be difficult because the drugs used are so permeable that only cell average partition coefficients could be obtained. Partition coefficients were estimated using 0.1 μm extruded unilamellar liposomes whose lipid compositions mimic, in a very simple way, the lipid compositions of the respective membrane monolayers. For the three drugs tested, the ratio of partition coefficients scaled roughly as $K_{BO} \approx K_{PC}/3$ and $K_{AO} \approx K_{PC}/10$. This scaling was used for the model data shown. However, because the scaling was rough, all of the simulations were also done with $K_{BO} = K_{AO} = K_{PC}$. The conclusions were the same, i.e., Figs. 8 and 9 looked the same. The scaling only changes absolute values of steady state parameters, but not the correlations.

[g] Mean value for the drug binding constant from inner apical membrane monolayer to P-gp.

model and analysis (24). Discussion of how the values in the table make considerable sense for P-gp function and structure can be found in Ref. (24). In our simulations, these two parameters are held fixed at the values shown.

This leaves four kinetically significant parameters characterizing individual substrate interaction with the confluent cell monolayer and P-gp, all of which are sensitive to the membrane composition and/or morphology:

(1) $k_2T(0)$, which is the true molecular membrane V_{max} of the substrate efflux by P-gp. Because $T(0)$ is assumed to be substrate independent, the efflux rate constant k_2 is substrate specific.

(2) K_B, which is the binding constant of the substrate to P-gp from the inner monolayer of the apical membrane.

(3) K_{PC}, which is the partition coefficient of the substrate between the inner monolayer of the apical membrane and the cytosol of the cell. The product of $K_{PC}K_B$ is the binding constant to P-gp relative to the cytosolic concentration of substrate. The two other partition coefficients, K_{BO}, between the basolateral chamber and the outer basolateral membrane monolayer, and K_{AO}, between the apical chamber and the outer apical membrane monolayer (see Fig. 1), are also fitted independently. However, we found that they roughly scale with K_{PC}, as explained in the legend to Table I (24). We have used this scaling to simplify the calculations, but we show below that the particular scaling does not alter any conclusions.

(4) P, which is the passive permeability coefficient of the substrate through the confluent cell monolayer, i.e., when P-gp is inhibited. For these simulations, we treat the cells as static permeability barriers, so that P is constant in time and the same in both directions. Reality is more complex. We found transients in the passive permeability coefficients which depended on the substrate and upon which cell membrane faced the donor chamber, i.e., apical or basolateral (23). To accurately fit the P-gp transport parameters, these transients had to be subtracted from the total transport. Here, for simplicity, these transients will be ignored because their inclusion would make the analysis more complex without affecting any of our conclusions.

The steady-state equation for the Michaelis–Menten reaction can be written as:

$$V(\tau) = \frac{V_{max} S^{\beta}}{K_M^{\beta} + S^{\beta}} \tag{2}$$

where S is the initial subst1rate concentration and V is the substrate transport velocity in the steady-state period, denoted as some time τ. When the Eadie–Hofstee plot is curved, the β in Eq. (2) is the simplest way to "fit" the curvature to obtain a better estimate for K_m. Note that in this definition, when $S = K_m$, then $V = 0.5V_{max}$, as is the textbook version.

Clearly, transport through a confluent cell monolayer is more complex than enzyme activity in aqueous solution, for which the Michaelis–Menten steady-state analysis was developed. However, the fitting of transport data using the steady-state equations is simple, and the steady-state kinetic equations are very elastic, i.e., they can fit many hyperbolic data sets quite well. Many sigmoidal data sets can be fitted by adding the "Hill" coefficient β. Unfortunately, having an r^2 value or correlation coefficient near 1, or a nonlinear

equivalent, does not mean that the fitted parameters are physically meaningful.

Calling. β a Hill number or coefficient suggests that its value is an estimate for the number of binding sites on the transporter. We will use the β coefficient to give the steady-state analysis the best opportunity to fit the K_m for the P-gp mediated transport data. Despite the fact that the model data are simulated for a P-gp with a single binding site, we will see below that for the confluent cell monolayer system, $\beta > 1$ is typical. In other words, for the confluent cell monolayer, $\beta > 1$ does not prove that P-gp has more than one binding site.

By dividing top and bottom of Eq. (2) by S, we can rearrange the equation into log-linear form:

$$\log\left\{\frac{V_{max}}{V(\tau)} - 1\right\} = -\beta \log\{S\} + \beta \log\{K_m\} \qquad (3)$$

Below, we will show how these equations can be used to best estimate V_{max} and K_m for the confluent monolayer system, using both experimental data and model data. Once the protocol is developed, we move to the real focus of this work, which is to assess the accuracy of the steady-state equations to predict the underlying molecular values.

RESULTS

The passive and active transport of 10 μM quinidine across the MDCKII-MDR1 cell monolayers is shown in Fig. 2. The passive permeability was determined in the presence of 2 μM GF120918, a potent inhibitor of P-gp (23,24,36,38). The nmol transported is symmetric (i.e., the same for B > A and A > B) over time when efflux is inhibited with GF120918 (closed symbols), as expected for a static passive barrier (23). The open symbols show the total transport when P-gp is active (without GF120918), with clear P-gp mediated activation of transport in the B > A direction and inhibition of transport in the A > B direction. Relative to passive permeability, the *activation* of B > A transport by P-gp, i.e., from the basolateral chamber to the apical chamber, illustrated by the length of the arrow aimed up, was always greater than the *inhibition* of A > B transport by P-gp, i.e., from the apical chamber to the basolateral chamber, illustrated by the length of the arrow aimed down. Remarkably, this simple test is diagnostic for there being only two barriers to active transport (24). If there were an additional kinetic barrier between the basolateral membrane inner monolayer and the apical membrane inner monolayer, e.g., substrates following a path through the cytosol, then the predicted shape of Fig. 2 would be just the opposite. The *activation* arrow would be shorter than the *inhibition* arrow (simulations not shown). The reason for this is that the additional barrier slows access of substrate to P-gp from the basolateral side, reducing activation, whereas transport from the apical side is further inhibited since the rate of drug escape to the basolateral membrane is reduced by the additional barrier, allowing more reuptake by P-gp. Other drugs have shown this "two-barrier" shape (19). Of course, this diagnostic can identify substrates for which there is a third barrier.

The activity of P-gp (nmol transported/h), i.e., V in the Michaelis–Menten equation [Eq. (2)], is typically obtained in the following way. We denote A:B > A as the transport into the apical chamber when the basolateral chamber is the donor. Then the total A:B > A transport (without P-gp inhibitor) minus the passive A:B > A transport (with P-gp inhibitor) is assigned to P-gp transport. We showed that this practice is accurate only if there is no backflow of substrate, which is more or less correct depending on the experiment (24). However, here we have followed the common practice for data analysis using the Michaelis–Menten steady-state equations and ignored backflux.

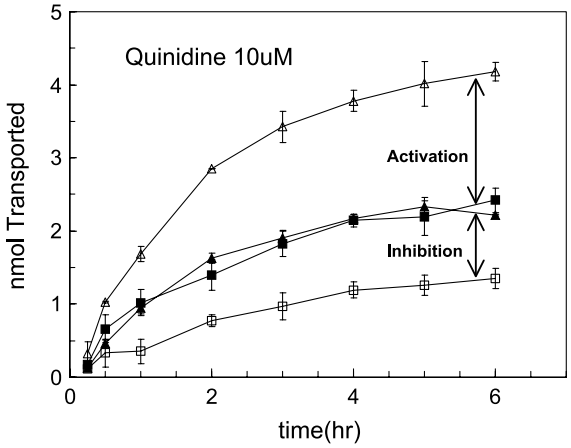

Fig. 2. The passive and active transport of quinidine across the monolayer of confluent MDCK cells is shown by nmol in the receiver chamber, over 6 h when the donor side begins with 10 μM quinidine. The filled symbols show passive permeability across the cell monolayer when the basolateral chamber was the donor side, B > A (▲), and when the apical side was the donor, A > B (■). The active transport by P-gp was completely inhibited by preincubation with 2 μM GF120918, added to both chambers. The empty symbols show the effect of P-gp on transport of quinidine across the cell monolayer, which occurs in the absence of GF120918. The fact that the activation of transport in the B > A direction over the passive transport by P-gp, the up arrow, is greater than the inhibition in the A > B direction, the down arrow, proves that there are only two barriers to transport, as explained in Tran *et al.* [24]. That is, transport through the cytosol is kinetically insignificant.

Figure 3 shows the Eadie–Hofstee plot for 0.3, 1, 3, 10, 20, and 30 μM quinidine. The slope, V, was taken from the 2-h data point of Fig. 2. This is a typical time for confluent cell monolayers. Choosing time points in the range of 1–4 h makes little difference, which will be shown below. However, choosing shorter time points would give incorrect results. The time point chosen to determine V must be somewhere within the steady-state phase of transport, defined as a constant amount of bound transporter, for the steady-state equations to have any validity. For a soluble enzyme, that can happen within sample mixing time. However, for the confluent cell monolayer, passive permeability through the donor membrane must occur first. For P-gp expressed in a confluent cell monolayer to achieve steady state required at least an hour for the three drugs we tested because of passive permeability through the membranes slows the binding reaction (24). A substrate with a higher passive permeability coefficient could be sampled at an earlier time, as shown below.

For a soluble Michaelis–Menten enzyme, the Eadie–Hofstee plot should be a straight line with a slope of $-K_m$ and a y-intercept of V_{max}. The fitted straight line in Fig. 3 has

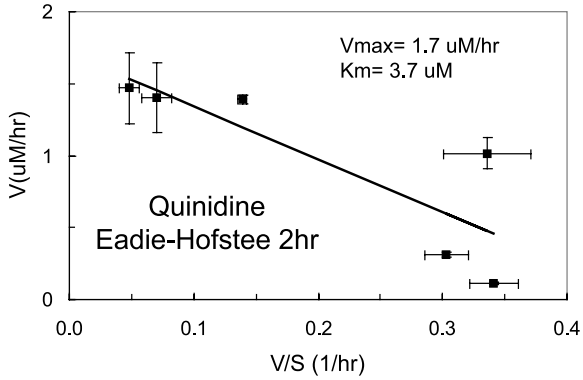

Fig. 3. Eadie–Hofstee plot of the quinidine data with V taken at 2 h, as explained in the text. Error bars are the standard deviation from triplicates. The straight line is the linear fit for all of the data. V_{max} = 1.7 μM/h and K_m = 3.7 μM. A curved fit is suggested but not certain because of the error. Quinidine concentrations were 0.3, 1, 3, 10, 20, and 30 μM.

K_m = 4 μM and V_{max} = 2 μM/h. Our fitted value for the K_m of quinidine is within a factor of 2 of the published value using the Caco-2 cell line (19). The Eadie–Hofstee plot for loperamide was similar (data not shown). Amprenavir showed no saturation up to 100 μM, i.e., no steady-state analysis was possible for this drug, despite the fact that the elementary rate constants could be fitted quite well (24).

The scatter in the data from the straight line is not a result of poor experiments. The Eadie–Hofstee plot in Fig. 3 appears curved, but this hypothesis would be difficult to defend statistically. To show that the plot is curved, we turn to model data, simulated using the mean values of the fitted parameters shown in Table I. The mass action differential equations used to simulate the model data are given in Tran *et al.* (24). The parameters in Table I for quinidine gave good fits for the transport of quinidine from 15 min to 6 h (24), so it is no surprise that the Eadie–Hofstee plots generated from the simulation would fit the data points shown in Fig. 3 (data not shown).

Figure 4 shows the Eadie–Hofstee plot for these model data, without error, and it is obviously curved. Only at high quinidine concentrations, where $V/S \rightarrow 0$, does the curve straighten toward the correct V_{max}, i.e., the value calculated from the parameters used in Table I. The same behavior was found for model data for loperamide and amprenavir (simulations not shown). Interestingly, the amprenavir model data only started showing saturation only above 150 μM, which we could not achieve experimentally.

One consequence of fitting V_{max} using linear regression of all of the data points would be to overestimate the V_{max}. For the confluent monolayer expression system, V_{max} should be estimated using only the highest substrate concentrations available. For model data mimicking quinidine, V_{max} = 1.17 μM/h (Fig. 4). This is closer to the value for the quinidine data in Fig. 3, when only the highest three concentrations are used there. Of course, this protocol works for a transporter with a single binding site or multiple independent sites. More complex transporters would require a more sophisticated analysis, but it is unlikely that the basic conclusions we reach here would change. It is worth noting here that the curvature of the Eadie–Hofstee plot is not a result of complicating effects, such as self-inhibition, because the model does not include them.

The primary cause of the curvature in the Eadie–Hofstee plot is the passive permeability. At low quinidine concentrations, the fraction of P-gp bound after 2 h is much less than what would be predicted simply from the drug-binding constant to a soluble enzyme because a true steady state has not yet been reached (simulation not shown).

Figure 5 shows the Eadie–Hofstee plots for model data mimicking quinidine using the elementary parameters from Table I, except that the passive permeability coefficient is varied from 20 to 1,000 nm/s. P = 1,000 nm/s is likely to be an upper bound for real drugs, and the graph is fairly straight. As the passive permeability coefficient decreases, the Eadie–Hofstee plot becomes more curved. When the passive permeability coefficient is 20 nm/s, the plot is straight again, but only the unsaturated part of the curve is shown. A longer incubation time, exceeding 4 h, would be needed to achieve a reasonable estimate for V_{max} with such small passive permeability coefficients.

Another result in Fig. 5 is that the V_{max} decreases as the passive permeability coefficient increases. Simulations have shown that at least 80% of the P-gp must be bound at the incubation time before the sharp left turn in the Eadie–Hofstee plot occurs, moving from small to higher substrate concentrations. That is, at least 80% of the P-gp must be bound to substrate in order for the correct value of V_{max} to be estimated. In our simulations, if we had used substrate concentrations greater than 100 μM and incubation times exceeding 4 h, straighter lines would have appeared. However, such conditions have not been used for these cell systems and P-gp. The results show that steady-state equations, like Eadie–Hofstee, convolve the passive permeability coefficient into the V_{max} parameter.

In order for the Eadie–Hofstee plot to yield realistic estimates for K_m, the curvature of the plot must be taken into account. The simplest way to allow for curvature in the Eadie–Hofstee plot is to use the β parameter in Eqs. (2) and (3). The meaning of β in terms of elementary P-gp parameters for these simulations is unclear, but it does not

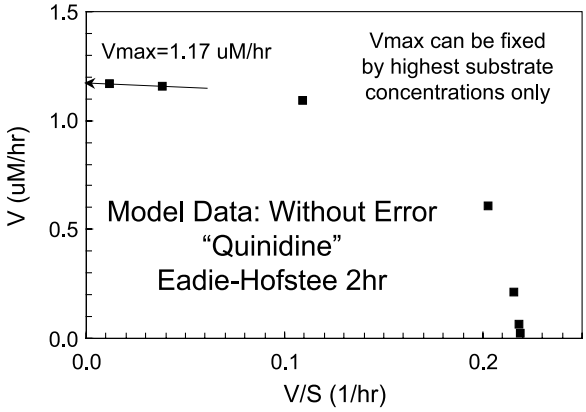

Fig. 4. Eadie–Hofstee plot of model data, from simulations, using the quinidine elementary parameters in Table I with V taken at 2 h. Because these are model data, there are no error bars. Substrate concentrations were 0.3, 1, 3, 10, 30, and 100 μM, which is used for all subsequent simulations. V_{max} = 1.17 μM/h is extrapolated using only the largest two substrate concentrations.

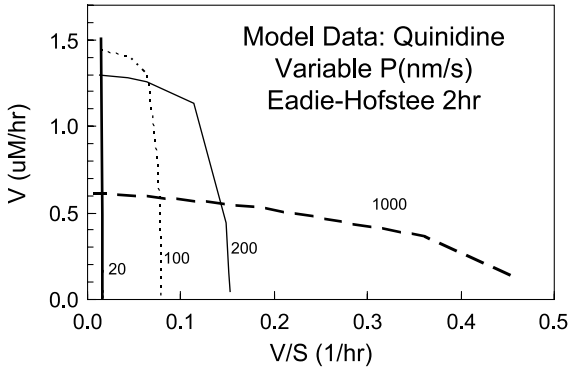

Fig. 5. Eadie–Hofstee plot of model data using the quinidine elementary parameters in Table I, except that the passive permeability coefficient is varied from 20 to 1,000 nm/s. V taken at 2 h.

represent the number of binding sites because the simulations used only one binding site.

Figure 6 shows the plot of the model data from Fig. 4 fitted using Eq. (3). V_{max} was fixed at 1.2 μM/h at the largest two substrate concentrations in Fig. 4. Then K_m and β can be fitted by Eq. (3). Although the straight line fits the model data quite well, there is a slight serpentine curvature in the model data, which shows that β alone cannot explain all of the curvature observed in the Eadie–Hofstee plots. Now we obtain K_m = 2 μM, somewhat smaller than the data in Fig. 3, and β = 1.5.

Figure 7 shows the Michaelis–Menten plot of the model quinidine data from Fig. 4. Clearly, the standard Michaelis–Menten plot, Eq. (2) with β ≡ 1, does not fit as well as using the fitted β. Of course, an extra fitting parameter is used, so the fit should be better. The quinidine data were fitted the same way, and both experimental and model data agreed quite well on V_{max}, K_m, and β, as shown in Table II. This protocol has demonstrated that the elementary parameters for quinidine fitted to the experimental transport curves generated over 6 h (24) can simulate the Eadie–Hofstee plots of the quinidine data. When the same analysis is applied to loperamide, we obtain the same basic results, except that β ~ 1 (data not shown, see Table II for the results). For

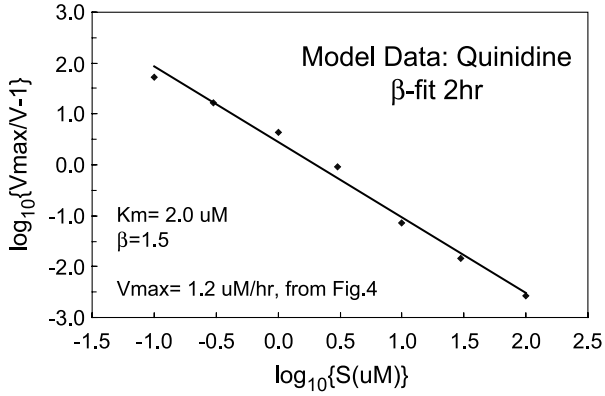

Fig. 6. The fit of model data from the quinidine elementary parameters in Table I by Eq. (3). V_{max} = 1.17 μM/h is extrapolated only from the largest two concentrations used (Fig. 4). This gives K_m = 2.0 μM and β = 1.5. Because the simulations had only one substrate binding site, the fact that β > 1 shows that it is not a Hill coefficient, just the simplest way to allow the Eadie–Hofstee plot to be curved.

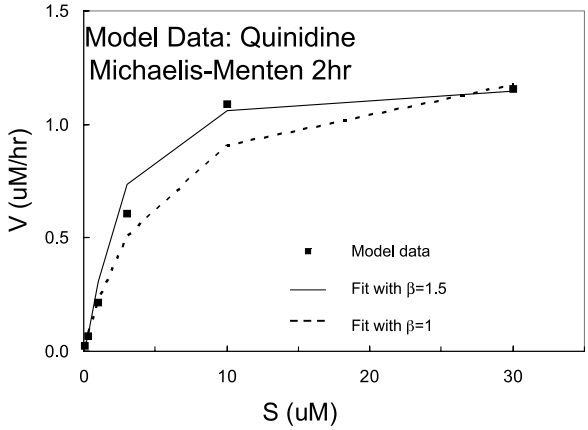

Fig. 7. Michaelis–Menten plots for Eq. (2) for model data using the quinidine parameters from Table I. V taken at 2 h. The solid lines use with β fitted (Table II), whereas the dashed line uses β fixed at 1.

amprenavir, because the data showed no saturation, as mentioned above, the simulated Eadie–Hofstee plots could not be compared with experimental data. However, model data using the amprenavir elementary parameters from Table I gave a β = 1.5, like quinidine (data not shown).

We noted above that the time point chosen for the Eadie–Hofstee plot would affect the steady-state parameter estimates. Table II shows the results. Based on the agreement in K_m estimates, it seems for quinidine that 2 h or longer is needed for the steady-state conditions to apply. Note for the model data that, as expected, V_{max} and K_m decreased as the incubation time increased. It must be reiterated that taking the velocity term $V(\tau)$ at earlier time points would reflect the passive permeation kinetics more than the P-gp efflux.

We now reach the real goal of this work. The final simulations addressed the question of how well the steady-state parameters derived from the Eadie–Hofstee analysis of model data correlate with the elementary parameters used to simulate the model data. To make these simulations physiologically relevant, the elementary parameters were limited to ranges found for amprenavir, quinidine, and loperamide (denoted as simulation range in Table I). For each parameter range, a grid was formed to cover each decade of the range with 3 points. For example, the range covered for $k_2T(0)$ was 1×10^{-4} to 1×10^{-2} (M/s), and the grid was [1×10^{-4}, 2×10^{-4}, 5×10^{-4}, 1×10^{-3}, ..., 1×10^{-2}].

All possible combinations of elementary parameters were used, generating 2,335 different elementary parameter combinations, with each parameter vector signifying a different "virtual" substrate. Each initial vector of parameters

Table II. Summary of Fits to Quinidine and Simulations

Incubation time (h)	V_{max} (μM/h)	K_m (μM)	β
1	1.4 (1.4)	7.8 (2.7)	1.1 (1.5)
2	1.5 (1.2)	2.2 (2.0)	1.4 (1.5)
4	1.0 (0.9)	1.8 (2.0)	1.3 (1.5)

The fitted V_{max}, K_m, and β values, using Eq. (3), are shown as a function of incubation time for quinidine and, in parentheses, for model data without error using the elementary parameters for quinidine shown in Table I.

was used for numerical integration of the mass action reactions with initial substrate concentrations of 0.1, 0.3, 1, 3, 10, 30, and 100 μM, which is the range we used in Tran *et al.* (24). Eadie–Hofstee plots of the model data were constructed to obtain V_{max} from the two highest substrate concentrations, with β = 1. Then Eq. (3) was used to fit K_m and β.

The fittings were culled to remove poor fits because of the limited substrate concentration range used. Fits were rejected when the V for the highest substrate concentration (100 μM) was smaller than 70% of the predicted V_{max} because the extrapolation was less accurate. This removed about 40% of the "virtual substrates". Choosing a higher cutoff, e.g., 80%, did not affect our conclusions and could not be justified relative to typical experimental procedure, i.e., the plots looked straight. The remaining fits showed no other obvious anomalies.

Our value for $k_2T(0)$ uses a $T(0)$ calculated from the volume of the inner apical monolayer, denoted V_{AO}, whereas V_{max} for a soluble enzyme refers to the enzyme concentration in the entire aqueous phase. We transformed the molecular $k_2T(0)$ to the value it would take as a "water-soluble" enzyme dispersed throughout both the Costar Transwell wells, i.e.,

$$V_{max\_mol} = k_2T(0)^*V_{AO}/V_T \quad (4)$$

where V_{AO} is the volume of the inner apical monolayer of all the cells in the monolayer, estimated at 0.5 nL in Tran *et al.* (24), but used exactly here for the simulations, and $V_T = 2$ mL is the total volume of the wells, 1.5 mL basolateral and 0.5 mL apical. The units are also transformed from M/s to μM/h.

Figure 8 shows the plot of the fitted V_{max} *vs.* V_{max_mol}, the membrane molecular value. The two are very well correlated, with slope of 1 on the log–log plot. For a given V_{max_mol}, the fitted values for V_{max} varied because of different passive permeability coefficients P. As P decreased, V_{max} increased because P-gp was less saturated at 2 h, and V_{max} is overestimated because of the curvature of the Eadie–Hofstee plot. Thus, for a given V_{max}, there is a 2- to

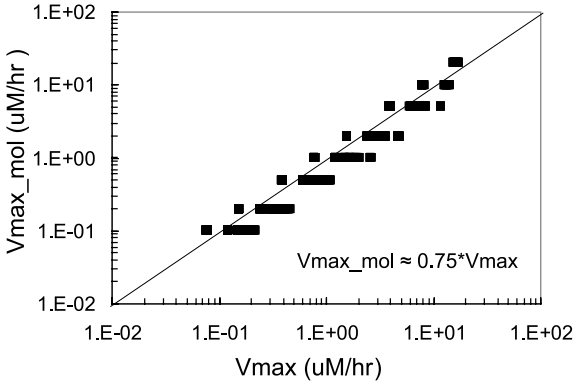

Fig. 8. Correlation of fitted V_{max} values, using Eq. (4), with V_{max_mol}, defined by Eq. (4), which is simply the transformation of $k_2T(0)$ to the value which P-gp would have as a soluble enzyme "dispersed" into the 2-mL transport chamber. For a grid of elementary parameters for 2,335 "virtual" substrates, defined by the last row of Table I, model data were simulated and then fitted to Eq. (3) as described in the text. After culling about 1,000 poor fits, the remaining 1,338 V_{max}/V_{max_mol} pairs are shown.

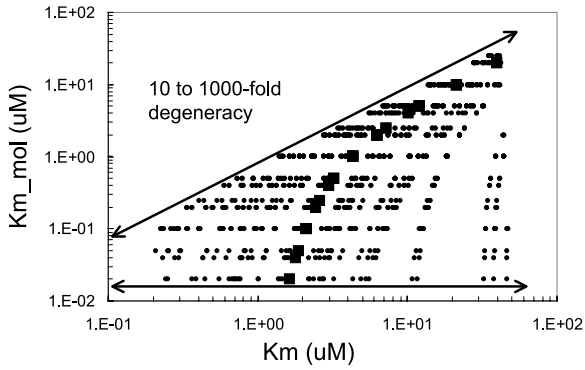

Fig. 9. Correlation between the fitted K_m and the elementary molecular K_{m_mol}, defined by Eq. (6), using the same model data as in Fig. 8. Obviously, there are many values of K_{m_mol} that give the same K_m, so the correlation is very poor. However, this plot is formed by families of curves, each one defined by a particular pair of values for the passive permeability coefficient, P, and the membrane molecular maximum efflux rate, $k_2T(0)$. The quinidine lineage of the family is shown by the large black points.

3-fold uncertainty in the molecular V_{max_mol}. This strong correlation could be anticipated because V_{max} is the maximal efflux rate, which is influenced only by the passive permeability and not substrate binding constants or partition coefficients.

The linear regression of V_{max_mol} *vs.* V_{max} in Fig. 8 gave an approximate relation of:

$$V_{max\_mol} \approx 0.75^*V_{max} \quad (5)$$

The factor of 0.75 comes from the intercept of the log–log plot. Thus, from the fitted V_{max}, one can estimate the molecular V_{max_mol} to within a factor of 2–3.

The situation for K_m is more complicated. Fig. 9 shows the plot for the fitted K_m *vs.* the aqueous version of the molecular value, i.e.,

$$K_{max\_mol}\,(\text{uM}) = 10^6*(k_2 + k_r)/(k_1*K_{PC}) \quad (6)$$

The solid double-arrowed lines show the range of a K_{m_mol} for a fitted K_m, both bottom and top. Although the fitted K_m is an upper bound for the K_{m_mol}, there is no other correlation. A fitted K_m of the order of 0.1 μM only specifies a 10-fold range of possible K_{m_mol} values, whereas a fitted K_m of the order of 10 μM only specifies 1,000-fold range of possible K_{m_mol} values. Actually, the real ranges are even larger. Following the arrows in Fig. 9 to smaller nM K_m values, it would seem that when the fitted K_m is about 50 nM, then K_{m_mol} would be about the same value. This is an artifact of restraining our simulations to the grid defined by amprenavir, loperamide, and quinidine parameters. When parameter values outside the range shown in Table I were used to obtain 10-fold smaller K_{m_mol} values, i.e., larger K_B and smaller k_2 values, then the lower bound of the fits for possible K_{m_mol} values was 10-fold smaller than seen in Fig. 9, ~1 nM. Thus, there is no convergence and perhaps no lower bound. We could extend our simulations to examine this, but then we would no longer know whether we were using physiologically relevant parameters.

Figure 9 was created using simulated data without experimental error. Close examination shows that K_m is related to K_{m_mol} by a family of curves. Each curve is defined by a particular pair of values for the passive permeability coefficient and the $k_2T(0)$. For example, the quinidine lineage curve [P = 300 nm/s and $k_2T(0)$ = 0.001 M/s] is highlighted by the large black squares in Fig. 9. The curve itself is a result of different values for the substrate binding constant, K_B, and inner apical membrane partition coefficient, K_{PC}. In fact, the curve depends only on the product $K_{PC}K_B$, which would be the binding constant measured from the concentration of substrate in the cytosol of the cell (i.e., the aqueous value of the binding constant). So there is a mathematical 1–1 relationship between K_m and K_{m_mol}, which in theory could be used to find the right K_{m_mol} given K_m and the other parameters.

However, this mathematical relationship would be useful only if it is not too sensitive to typical experimental error. To test this, we repeated the simulations and fittings with 5 and 10% normally distributed "experimental" error added to the transported concentrations. Each simulation yielded about 1,300 good Eadie–Hofstee plots out of the 2,335 initial vectors. Unfortunately, the family of curves became too blurred to follow any lineage, and no further analysis was possible.

DISCUSSION

We have investigated the correlation between the elementary kinetic parameters that define the transport and the Michaelis–Menten steady-state parameters fitted to that transport for a confluent monolayer of MDCKII-hMDR1 cells, which overexpress P-gp. For transport of amphipathic compounds across a confluent monolayer of cells, there are two inherent problems with the Michaelis–Menten analysis. First, access of substrate to P-gp depends on passive permeability, which is not part of the Michaelis–Menten analysis. It takes longer times in the cell monolayer system to reach steady state, where the math is most valid, than in the more commonly used cell or membrane vesicle suspensions. The second inherent problem is that there are many elementary parameters that govern transport, and their values are convolved into the steady-state parameters of V_{max} and K_m.

In Tran *et al.* (24), we were able to determine the elementary parameters for three drugs which are good P-gp substrates (Table I). With this knowledge, we have been able to assess the quality of the correlation theoretically, i.e., where we know the answer, within a domain of the elementary parameter space we know to be physiologically relevant.

A grid of 2,335 "virtual" substrates was created, whose values for passive permeability coefficients, maximum efflux rate constant, binding constant, and partition coefficient are approximately bounded by the values found for the three drugs, as shown in Table I. Because the three drugs studied yielded the same value for the surface density of efflux active P-gp, $T(0)$, and for the association rate constant, k_1(24), those values were used for the simulation.

The substrate concentrations ranged from 0.1 to 100 μM, which are typical concentrations used in transport experiments. This meant that some parameter vectors would have the wrong substrate concentration range to yield good fits to the Eadie–Hofstee plot. We found that all of these cases could be identified, and discarded, when V at the largest substrate concentration, V(100 μM), was less than 70% of the predicted V_{max}. This removed about 40% of the cases. The remaining 1,338 "virtual" substrates yielded reasonable-looking Eadie–Hofstee plots, based on regression coefficients, i.e., there was no reason to reject them.

The next question was how to compare fitted V_{max} and K_m values to the underlying molecular values. When the molecular value of $V_{max} = k_2T(0)$ was converted to the value it would be if P-gp were "resuspended as a soluble enzyme" into the aqueous volume of the transport apparatus, defined as V_{max_mol} in Eq. (4), the correlation with V_{max} was rather good. The correlation coefficient was $r^2 \approx 1$ and the slope was 1. To within a factor of 2–3, $V_{max\_mol} \approx 0.75V_{max}$. This means that the fitted V_{max} can roughly, but consistently, estimate the molecular values of $k_2T(0)$. The range was due to the range of the passive permeability coefficients used, which is not part of the classical V_{max} definition.

The story for K_m is more complex, basically because more of the elementary parameters that really drive transport are convolved into the fitted K_m. This is unfortunate because this parameter is the simplest estimate of the substrate binding constant to P-gp, *in vitro* and *in vivo*. Figure 9 shows that as the fitted value of K_m increases from 0.3 to 10 μM values, typical for current drugs and P-gp, the range of elementary K_{m_mol} values that could yield that fitted K_m increases from 10- to 1,000-fold. This means that the fitted K_m from experimental data cannot be expected to have any useful correlation with $K_{m\_mol} = (k_r + k_2)/k_1$. Thus, two drugs with identical steady-state K_m's for this cell line are likely to have very different values *in vivo*. The elementary kinetic parameters generate the *in vivo* phenomenological values for V_{max} and K_m, based on the local membrane environment.

For the sake of completeness, it is worth noting that the relationship between the phenomenological K_m and the molecular K_{m_mol} is not really random. They are associated by a family of curves. For the quinidine lineage, shown by the large black points in Fig. 9, the family of points all have P = 300 nm/s and $k_2T(0) = 10^{-3}$ M/s. The product of $K_{PC}K_B$ for the "virtual substrates" comprising this curve determines its shape. $K_{PC}K_B$ is the binding constant of the substrate to P-gp, relative to the aqueous phase.

Unfortunately, the delineated curves are calculated using model data without error, which is not experimentally attainable. We repeated all the simulations, adding 5 and 10% normally distributed error with the MATLAB randn function, and found that the individual points within a lineage moved adequately to become interwoven with other lineages. The curves blur beyond recognition when the data have error. Thus, when data have error, there is no way to estimate the value of K_{m_mol} from the fitted K_m.

CONCLUSION

Extrapolation of P-gp substrate interactions of the confluent monolayer system to *in vivo* can be performed with far greater confidence when the elementary parameters

are known. This requires the fitting of transport kinetics over multiple time points, as we did in Tran *et al.* (24). Our analysis of P-gp transport is more complex than previous kinetic analyses because we did not impose the steady-state Michaelis–Menten equations onto the data. P-glycoprotein active transport has more than six kinetically important parameters, which become convolved into the V_{max} and K_m of the Michaelis–Menten equation. We believe that this convolution will ultimately hinder the resolution of P-gp mechanism. In Tran *et al.* (24), we took nine time points, from 6 min to 6 h, for at least six substrate concentrations to fit the elementary rate constants. Here, we have shown that six substrate concentrations and one incubation time cannot yield reliable estimates of the molecular K_{m_mol}. We are now optimizing this analysis to discover how many and which time points and substrate concentrations are required to fix the elementary parameters with adequate accuracy.

REFERENCES

1. K. S. Lown, R. R. Mayo, A. B. Leichtman, H. L. Hsiao, D. K. Turgeon, P. Schmiedlin-Ren, M. B. Brown, W. Guo, S. J. Rossi, L. Z. Benet, and P. B. Watkins. Role of intestinal P-glycoprotein (mdr1) in interpatient variation in the oral bioavailability of cyclosporine. *Clin. Pharmacol. & Therap.* **62**(3):248–260 (1997).
2. A. H. Schinkel. Pharmacological insights from P-glycoprotein knockout mice. *Int. J. Clin. Pharmacol. & Therap.* **36**(1):9–13 (1998).
3. L. B. Goh, K. J. Spears, D. Yao, A. Ayrton, P. Morgan, W. C. Roland, and T. Friedberg. Endogenous drug transporters in *in vitro* and *in vivo* models for the prediction of drug disposition in man. *Biochem. Pharmacol.* **64**:1569–1578 (2002).
4. P. Borst and R. O. Elferink. Mammalian ABC transporters in health and disease. *Ann. Rev. Biochem.* **71**:537–592 (2002).
5. M. M. Gottesman. Mechanisms of cancer drug resistance. *Annu. Rev. Med.* **53**:615–627 (2002).
6. S. V. Ambudkar, C. Kimchi-Sarfaty, Z. E. Sauna, and M. M. Gottesman. P-glycoprotein: from genomics to mechanism. *Oncogene* **22**:7468–7485 (2003).
7. A. E. Senior, M. K. Al-Shawi, and I. L. Urbatsch. The catalytic cycle of P-glycoprotein. *FEBS Lett.* **377**(3):285–289 (1995).
8. H. W. van Veen, A. Margolles, M. Muller, C. F. Higgins, and W. N. Konings. The homodimeric ATP-binding cassette transporter LmrA mediates multidrug transport by an alternating two-site (two-cylinder engine) mechanism. *EMBO J.* **19**:2503–2514 (2000).
9. C. Martin, G. Berridge, C. F. Higgens, P. Mistry, P. Charlton, and R. Callaghan. Communication between Multiple Drug binding sites on P-glycoprotein. *Mol. Pharmacol.* **58**:624–632 (2000).
10. C. Martin, C. F. Higgins, and R. Callaghan. The vinblastine binding site adopts high- and low-affinity conformations during a transport cycle of P-glycoprotein. *Biochemistry* **40**:15733–15742 (2001).
11. Q. Qu, J. W. Chu, and F. J. Sharom. Transition state P-glycoprotein binds drugs and modulators with unchanged affinity, suggesting a concerted transport mechanism. *Biochemistry* **42**:1345–1353 (2003).
12. M. K. Al-Shawi, M. K. Polar, H. Omote, and R. A. Figler. Transition state analysis of the coupling of drug transport to ATP hydrolysis by P-glycoprotein. *J. Biol. Chem.* **278**:52629–52640 (2003).
13. S. H. Jang, M. G. Wientjes, and J. L.-S. Au. Interdependent effect of P-glycoprotein-mediated drug efflux and intracellular drug binding on intracellular paclitaxel pharmacokinetics: Application of computational modeling. *J. Pharmacol. Exp. Therap.* **304**:773–780 (2003).
14. T. W. Loo, M. C. Bartlett, and D. M. Clarke. Substrate-induced conformational changes in the transmembrane segments of human P-glycoprotein. Direct evidence for the substrate-induced fit mechanism for drug binding. *J. Biol. Chem.* **278**(16):13603–13606 (2003).
15. I. L. Urbatsch, G. A. Tyndall, G. Tombline, and A. E. Senior. P-glycoprotein catalytic mechanism: Studies of the ADP-vanadate inhibited state. *J. Biol. Chem.* **278**(25):23171–23179 (2003).
16. F. Tang, K. Horie, and R. T. Borchardt. Are MDCK cells transfected with the human MRP2 gene a good model of the human intestinal mucosa? *Pharm. Res.* **19**:765–772 (2002a).
17. F. Tang, K. Horie, and R. T. Borchardt. Are MDCK cells transfected with the human MDR1 gene a good model of the human intestinal mucosa? *Pharm. Res.* **19**:773–779 (2002b).
18. M. D. Troutman and D. R. Thakker. Novel experimental parameters to quantify the modulation of absorptive and secretory transport of substrates by P-glycoprotein in cell culture models of intestinal epithelium. *Pharm. Res.* **220**:1210–1224 (2003a).
19. M. D. Troutman and D. R. Thakker. Efflux ratio cannot assess P-glycoprotein-mediated attenuation of absorptive transport: Asymmetric effect of P-glycoprotein on absorptive and secretory transport across Caco-2 cell monolayers. *Pharm. Res.* **20**:1200–1209 (2003b).
20. A. Seelig and E. Gatlik-Landwojtowicz. Biophysical characterization of inhibitors of multidrug efflux transporters: Their membrane and protein interactions. *Med. Chem. (Minirev.)* **5**(2):135–151 (2005).
21. H. Omote, R. A. Figler, M. K. Polar, and M. K. Al-Shawi. Improved energy coupling of human P-glycoprotein by the glycine 185 to valine mutation. *Biochemistry* **43**:3917–3928 (2004).
22. G. Tombline, G. Lori, A. Bartholomew, G. A. Tyndall, K. Gimi, I. L. Urbatsch, and A. E. Senior. Properties of P-glycoprotein with mutations in the "catalytic carboxylate" glutamate residues. *J. Biol. Chem.* **279**:46518–46526 (2004).
23. T. T. Tran, A. Mittal, T. Gales, B. Maleeff, T. Aldinger, J. W. Polli, A. Ayrton, H. Ellens, and J. Bentz. An exact kinetic analysis of passive transport across a polarized confluent MDCK cell monolayer modeled as a single barrier. *J. Pharm. Sci.* **93**:2108–2123 (2004).
24. T. T. Tran, A. Mittal, T. Aldinger, J. W. Polli, A. Ayrton, H. Ellens, and J. Bentz. The elementary mass action rate constants of P-gp transport for a confluent monolayer of MDCKII-hMDR1 cells. *Biophys. J.* **88**:715–738 (2005).
25. W. D. Stein. Kinetics of the multidrug transporter (P-glycoprotein) and its reversal. *Physiol. Rev.* **77**(2):545–590 (1997).
26. N. F. H. Ho, P. S. Burton, R. A. Conradi, and C. L. Barsuhn. A biophysical model of passive and polarized active transport processes in Caco-2 cells: Approaches to uncoupling apical and basolateral membrane events in the intact cell. *J. Pharm. Sci.* **84**(1):21–27 (1995).
27. N. F. H. Ho, T. J. Raub, P. S. Burton, C. L. Bausuhn, A. Adson, K. L. Audus, and R. Borchardt. Quantitative approaches to delineate and passive transport mechanisms in cell culture monolayers. In G. L. Amidon and P. I. Lee (eds), *Transport Processes in Pharmaceutical Systems*, Marcel Dekker, New York, 2000, pp. 219–316.
28. S. Doppenschmitt, H. Spahn-Langguth, C. G. Regardh, and P. Langguth. Role of P-glycoprotein-mediated secretion in absorptive drug permeability: An approach using passive membrane permeability and affinity to P-glycoprotein. *J. Pharm. Sci.* **88**:1067–1072 (1999).
29. S. Ito, C. Woodland, B. Sarkadi, G. Hockmann, S. E. Walker, and G. Koren. Modeling of P-glycoprotein-involved epithelial drug transport in MDCK cells. *Am. J. Physiol.-Renal Fluid Electrolyte Physiol.* **46**:F84–F96 (1999).
30. H. J. Kuh, S. H. Jang, M. G. Wientjes, and J. L. Au. Computational model of intracellular pharmacokinetics of paclitaxel. *J. Pharmacol. Exp. Ther.* **293**:761–770 (2000).
31. A. Ruth, W. D. Stein, E. Rose, and I. B. Roninson. Coordinate changes in drug resistance and drug-induced conformational transitions in altered-function mutants of the multidrug transporter P-glycoprotein. *Biochemistry* **40**:4332–4339 (2001).
32. M. Sasaki, H. Suzuki, K. Ito, T. Abe, and Y. Sugiyama. Transcellular transport of organic anions across a double transfected Madin–Darby Canine Kidney II cell monolayer expressing both human organic anion-transporting polypeptide (OATP2/SLC21A6) and multidrug resistance-associated protein 2 (MRP2/ABCC2). *J. Biol. Chem.* **277**:6497–6503 (2002).

33. F. J. Meyer-Almes and M. Auer. Enzyme inhibition assays using fluorescence correlation spectroscopy: A new algorithm for the derivation of kcat/KM and Ki values at substrate concentrations much lower than the Michaelis constant. *Biochemistry* **39**(43):13261–13268 (2000).
34. F. J. Sharom and P. D. Eckford. Reconstitution of membrane transporters. *Methods Mol. Biol.* **227**:129–154 (2003).
35. M. R. Lugo and F. J. Sharom. Interaction of LDS-751 with P-glycoprotein and mapping of the location of the R drug binding site. *Biochemistry* **44**:643–655 (2005).
36. J. W. Polli, S. A. Wring, J. E. Humphreys, L. Huang, J. B. Morgan, L. O. Webster, and C. S. Serabjit-Singh. Rational use of *in vitro* P-glycoprotein assays in drug discovery. *J. Pharmacol. & Exp. Ther.* **299**(2):620–628 (2001).
37. R. Evers, M. Kool, A. J. Smith, L. van Deemter, M. de Haas, and P. Borst. Inhibitory effect of the reversal agents V-104, GF120918 and Pluronic L61 on MDR1 Pgp-MRP1- and MRP2-mediated transport. *Br. J. Cancer* **83**:366–374 (2000).
38. F. Hyafil, C. Vergely, P. Du Vignaud, and T. Grand-Perret. *In vitro* and *in vivo* reversal of multidrug resistance by GF120918, an acridonecarboxamide derivative. *Cancer Res.* **53**:4595–4602 (1993).
39. C. Butor and J. Davoust. Apical to basolateral surface area ratio and polarity of MDCK cells grown on different supports. *Exp. Cell Res.* **203**:115–127 (1992).
40. S. Modok, C. Heyward, and R. Callaghan. P-glycoprotein retains function when reconstituted into a sphingolipid and cholesterol rich environment. *J. Lipid Res.* **45**:1910–1918 (2004).
41. J. Troost, H. Lindenmaier, W. E. Haefeli, and J. Weiss. Modulation of cellular cholesterol alters P-glycoprotein activity in multidrug-resistant cells. *Mol. Pharmacol.* **66**:1332–1339 (2004).